

Spin transport-induced damping of coherent THz spin dynamics in iron

L. Brandt,¹ R. Verba,² N. Liebing,¹ M. Ribow,¹ I. Razdolski,³
V. Tyberkevych,⁴ A. Slavin,⁴ G. Woltersdorf,¹ and A. Melnikov¹

¹*Martin Luther University Halle-Wittenberg,
Institute of Physics, Optics Group,
Von-Danckelmann-Platz 3, 06120 Halle*

²*Institute of Magnetism, Kyiv 03142, Ukraine*

³*Faculty of Physics, University of Bialystok, 15-245 Bialystok, Poland*

⁴*Department of Physics, Oakland University, Rochester, MI 48309, USA*

(Dated: July 28, 2021)

Abstract

We study the damping of perpendicular standing spin-waves (PSSWs) in ultrathin Fe films at frequencies up to 2.4 THz. The PSSWs are excited by optically generated ultrashort spin current pulses, and probed optically in the time domain. Analyzing the wavenumber and thickness dependence of the damping, we separate different contributions and demonstrate that at sufficiently large wave vectors k the damping is dominated by spin transport effects scaling with k^4 and limiting the frequency range of observable PSSWs. Although such contribution is known to originate in the spin diffusion, we argue that at moderate and large k the super-diffusive character of the spin transport again reduces the related damping term.

Understanding dissipation mechanisms is one of the most important problem of dynamical systems. Ferromagnetic materials exhibit a wide variety of dissipation processes which contribute to the total decay rate of a spin-wave mode depending on the material, static magnetization state, geometry, etc. [1, 2]. These processes include effects, such as 2-magnon scattering on imperfections [3–5], spin pumping into an adjacent nonmagnetic layers [6–8], and intrinsic Gilbert damping. The latter originates in magnon-phonon and magnon-electron interactions due to the spin orbit coupling and is usually the most important contribution to magnetic damping. It is well described within a phenomenological model[9] and leads to a dissipation term in the Landau-Lifshitz equation of magnetization motion in the form $\mathbf{T}_d = \alpha_G/M_s (\mathbf{M} \times \partial\mathbf{M}/\partial t)$ where the Gilbert damping parameter α_G is assumed to be constant. In metallic ferromagnets, where the magnetic damping is dominated by the magnon-electron interactions, this phenomenological description is well supported by ab-initio calculations [10–15]. The Gilbert model also rather well describes the damping in magnetic dielectrics for experiments performed in the microwave frequency range. One of the main assumptions of the Gilbert model is its locality, i.e. the assumption that the damping rate Γ_n of a spin-wave mode n depends only on the mode frequency ω_n and the mode precession ellipticity (described by the coefficient ϵ_n), $\Gamma_n = \alpha_G \epsilon_n \omega_n$ [16], but does not depend on the spatial structure of the mode. For exchange-dominated magnons the magnon frequency is $\omega_n \sim k_n^2$ and in the framework of the Gilbert model, the magnon damping rate (inverse magnon lifetime) is also $\Gamma_n \sim k_n^2$.

Kamberský was the first to point out, that the dissipation term in magnetization dynamics should also contain a non-local (wavenumber-dependent) contribution [11]. A phenomenological description of the "exchange contribution" to the dissipation term was introduced by Bar'yakhtar and it was shown that this contribution leads to a $\Gamma_n \sim k_n^4$ dependence of the damping rate [17, 18]. Much later, a process of spin diffusion was proposed as a microscopic mechanism of the non-local intrinsic magnetization damping [19–23]. Transverse spin diffusion leads to the enhancement of the effective Gilbert damping parameter $\Delta\alpha_n \sim k_n^2$, causing a $\Gamma_n \sim k_n^4$ dependence, as proposed in [21, 24, 25]. So far, the experimental verification of these theoretical predictions was rather limited. Indeed, most of the research work on the spin-wave damping was performed in the microwave frequency band for relatively long (sub-micron and larger wavelength) spin waves, where non-local damping effects are quite weak and difficult to identify. First attempts to study non-local effects in magnetic dissipation

were made by Nembach et al., who suggested that the experimentally observed mode- and size dependent damping in 100-nm-sized magnetic nanodots is related to the spin diffusion [26]. Later, a study of perpendicular standing spin wave (PSSW) modes with wavenumbers of up to $k_n < 0.12 \text{ nm}^{-1}$ demonstrated a k_n^2 -dependence of the effective Gilbert damping parameter [25]. However, the spin wave damping in the range of larger wavenumbers remains mostly unexplored. In this exchange-dominated region the experiments were mostly focused on the magnon dispersion, using neutron scattering and spin-polarized electron energy loss spectroscopy (SPEELS)[27–30].

In this letter, we study THz-frequency PSSW with large wavenumbers and frequencies of up to 2.4 THz in iron layers. In addition to shedding light on the dissipation of such THz spin waves, we identify a fundamental limit for the observation of the spin waves at which the damping rate becomes equal to the spin wave eigenfrequency, and the PSSWs become overdamped. Our results demonstrate that an exchange-driven spin diffusion mechanism plays the dominant role in the dynamic magnetization damping at sufficiently large wavenumbers, and that, most likely a different super-diffusive damping mechanism becomes dominant at even larger values of the spin wave wavenumbers.

For our experiments epitaxial Fe/Au/Fe(001) multilayers, as indicated in Fig. 1 (a), are prepared [32]. The measurements of the THz-frequency spin dynamics are based on the optical pump-probe technique developed in [33], and used in [34, 35]. The magnetization dynamics in a Fe wedge (collector) is excited by an ultrashort spin current pulse generated in the Fe emitter by a laser pump pulse. Spin waves are detected in the time domain by a probe pulse using the magneto-optical Kerr effect (MOKE). Importantly, a thick Au spacer layer blocks the pump beam (from the back side) and allows the excitation of the collector by a spin current pulse only (i.e. not optically). Note that the 70 nm thick Au spacer does not stretch the spin current pulses significantly, and the fs time resolution is maintained [36]. This experimental approach allows for systematic measurements of the frequencies and lifetimes of the PSSW modes vs. the thickness of the Fe collector using a single sample, where the PSSWs are excited via ultrashort spin transfer torque (STT) pulses.

In Fig. 1(b) an example of time-resolved polar MOKE rotation θ and ellipticity ε at 12 nm Fe collector is shown. The periodic signals with multiple frequencies indicate the excitation of several PSSW eigenmodes. By fitting these curves to a sum of damped cosine functions a set of lifetimes $\tau_n = \Gamma_n^{-1}$ and frequencies f_n for each PSSW eigenmode with

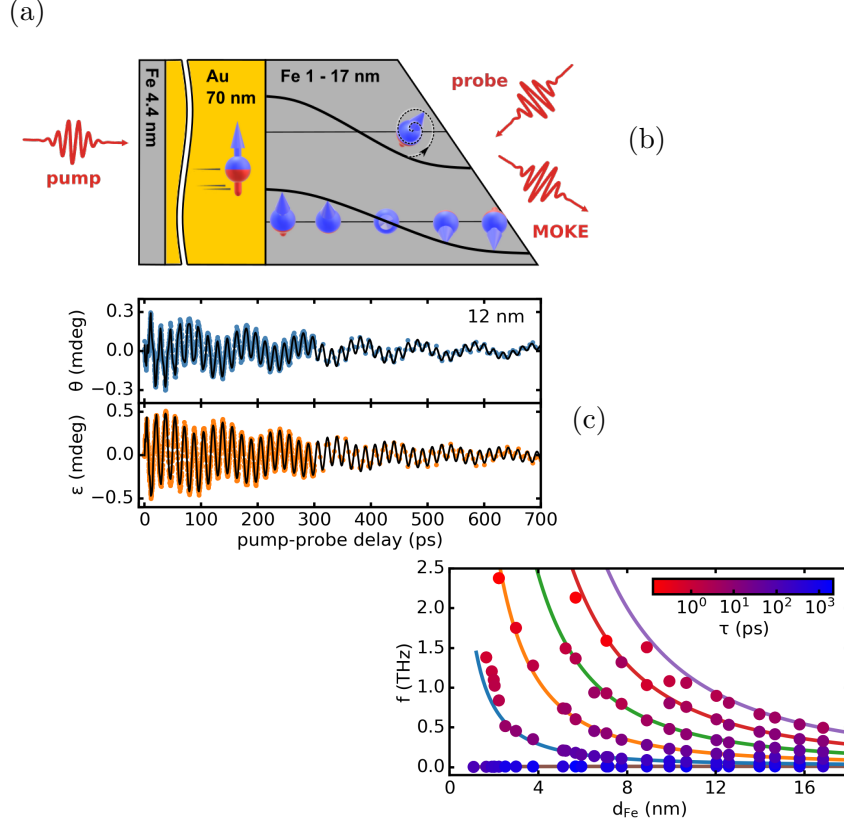


FIG. 1: (a) Sample layout and measurement geometry. (b) Exemplary time-resolved MOKE measurement (rotation θ and ellipticity ϵ) at 12 nm Fe collector thickness including the fit of damped cosine. (c) FMR and PSSW frequencies (y-axis) and lifetimes (color-code) obtained by fits to the time-resolved MOKE traces (as shown in (b)). The solid lines are a theoretical fit (see Supplemental Material [31]).

index n is obtained. The observed modes can be identified by a fit to the PSSW dispersion relation, while accounting for the magnetic anisotropy and the dependence of the exchange stiffness on the Fe thickness [31, 32]. The PSSW wavenumbers are well described by the relation $k_n = n\pi/d_{\text{Fe}}$ implying that there are no magnetically dead layers. The correct assignment of the PSSW wavenumbers is crucial for the analysis presented below. Up to 6 spin wave modes are observed (the ferromagnetic resonance (FMR) mode and 5 PSSW modes), depending on the collector thickness d . The maximum observed PSSW frequency is about $f_{\text{max}} = 2.4$ THz (Fig. 1(c)), which corresponds to the shortest observed wavelength $\lambda_{\text{min}} = 2.22$ nm.

Next, we discuss the dependence of the spin wave mode lifetime on the oscillation period $T_n = 1/f_n$, as it is shown in Fig. 2(a). It is evident that the data are well fitted by a

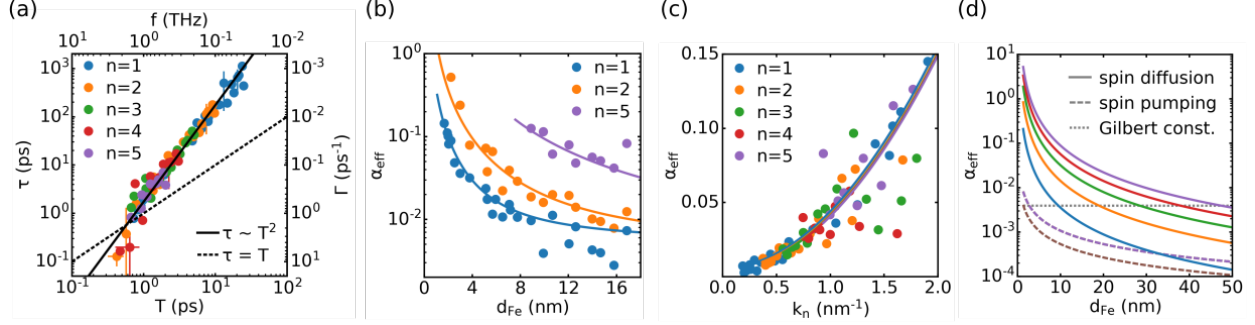


FIG. 2: (a) Double logarithmic plot of measured lifetimes τ (damping rate Γ) of PSSW modes vs. the mode oscillation period T (frequency f). Solid line represents the quadratic fit $\tau \sim T^2$ and dashed line represents the dependence $\tau = T$. (b) Effective damping for the first, second and fifth PSSW mode as a function of the Fe thickness. Points are the experimental data; solid lines are the fits to the data for all the modes performed using the model expression Eq. 1. For experimental data and the corresponding fits for $n=0$, $n=3$, $n=4$ see Supplemental material [31] (c) Effective damping for the first five PSSW modes as a function of the wavenumber k_n . The points are the experimental data, the lines are the fit to the data. (d) Most important terms in our model of the effective damping (Eq. 1) calculated as results of the fitting procedure, but for a broader range of Fe thicknesses. Note, that the volume and surface contributions are not shown [31].

$\tau_n \sim T_n^2$ dependence (solid line) corresponding to $\Gamma_n \sim k_n^4$ when $f_n \sim k_n^2$. We find that at $f = 1.8$ THz ($T = 0.56$ ps, see the intersection with the $\tau_n = T_n$ dashed line in Fig. 2(a)) the spin wave lifetime becomes smaller than the oscillation period, implying that the spin wave modes become overdamped. Above this critical frequency the PSSWs are hardly detectable. Accordingly, only very few data points obtained with rather large error bars can be extracted from the raw data between 1.8 and 2.4 THz.

For further analysis we will use an effective Gilbert damping parameter $\alpha_{\text{eff},n} = \Gamma_n / (\omega_n \epsilon_n) = (2\pi\tau_n f_n \epsilon_n)^{-1}$, which is more convenient for the comparison of relaxation rates between the different modes (here and below $\omega_n = 2\pi f_n$ is the mode angular frequency). The ellipticity-related coefficient ϵ_n was calculated [31] from the dispersion equation of the spin-wave modes [16, 32]. In the range of interest (above 100 GHz) the ellipticity parameter ϵ_n is very close to 1 [31]. The dependence of the effective damping parameter $\alpha_{\text{eff},n}$ on the Fe film thickness for all the observed modes is shown in Fig. 2(b) (see also Supplemental material [31]). It is clear, that the effective damping parameter strongly increases with the

mode number n and the inverse film thickness. To analyze these data, we use the following phenomenological model for the effective damping parameter in the non-local case:

$$\alpha_{\text{eff},n} = \alpha_G + \frac{\Gamma_{\text{nu}}}{\omega_n \epsilon_n} + \frac{G_{\text{nu}}}{\omega_n \epsilon_n d} + \frac{c_n \eta_s}{d} + \eta_{\perp} k_n^2. \quad (1)$$

The first term in this expression represents the intrinsic Gilbert damping constant, the next two terms describe the non-uniform resonance line broadening with volume contribution Γ_{nu} (due to volume defects) and surface contribution G_{nu}/d (due to surface defects and imperfections). The impact of the latter naturally scales inversely with the film thickness. The fourth term $\sim \eta_s$ describes the spin-pumping into the adjacent Au layer with the coefficient $c_n = 1$ for $n = 0$ and $c_n = 2$ for the higher modes [16]. The last term represents the k_n^2 -dependent exchange-driven contribution, which we attribute to spin transport.

The different contributions to the effective damping parameter $\alpha_{\text{eff},n}$ as described by Eq. (1) are obtained from the best joint fit of all 6 measured spin wave modes (FMR and 5 PSSWs). Owing to the high epitaxial quality of the sample, the volume contribution is negligible ($\Gamma_{\text{nu}} = (0.08 \pm 0.1) \cdot 10^{-3} \text{ ps}^{-1}$). The obtained value of the Gilbert damping constant $\alpha_G = (3.94 \pm 1.9) \cdot 10^{-3}$ is close to the standard value for Fe $\alpha_G = 0.0038$ [7]. The surface-driven broadening $\sim G_{\text{nu}}$ and the spin-pumping induced damping $\sim \eta_s$ have a similar magnitude, and are essential only for the $n = 0$ mode: $G_{\text{nu}} = (5.54 \pm 2.1) \text{ nm ps}^{-1}$, $\eta_s = (5.38 \pm 3.1) \text{ nm}$ (compare Fig. 2 (d) and Supplemental material [31]). Notably, they can be determined in the fitting procedure due to the fact that the surface contribution is frequency independent (while the contribution from the spin pumping is not). Moreover, the magnitude of the spin pumping contribution is in good agreement with the literature values for the Fe/Au system: $\eta_s \approx 3 \cdot 10^{-3} \text{ nm}$ [7, 37].

The observed effective damping $\alpha_{\text{eff},n}$ for the PSSW modes in the considered range of the Fe layer thickness is mainly k_n^2 -dependent. This becomes obvious from Fig. 2(c), where we show that the effective damping follows a $\alpha_{\text{eff},n} - \alpha_G \sim k_n^2$ dependence for all the PSSWs. This implies that the other contributions which are different for different modes at a given k (corresponding to different film thickness), are not important. For example, one can see in Fig. 2(d) that for Fe films with a thickness of less than 10 nm, already for the lowest PSSW mode with $n=1$ (blue line) the spin diffusion is the dominant damping mechanism. The k^2 dependence of the effective damping parameter describes the experimental data well up to $k \approx 1 \text{ nm}^{-1}$, corresponding to $f \approx 0.6 \text{ THz}$. At larger wavenumbers the magnetization

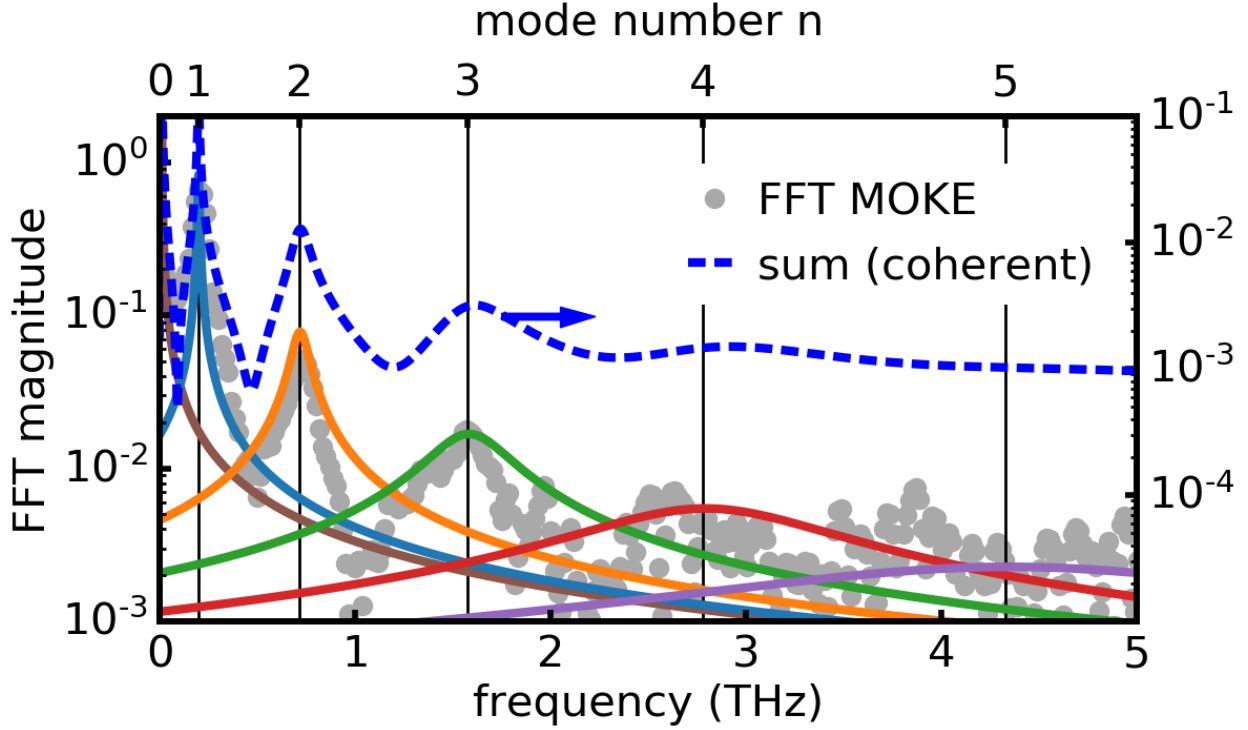


FIG. 3: FFT magnitude (dots) of the polar MOKE ellipticity measured at the 5.2 nm-thick Fe collector. Solid lines represent lorentzian lineshapes with equal peak areas calculated based on Eq. (1), the color code corresponds to that in Fig. 2. Dashed line shows scaled coherent sum of these modes. Vertical lines indicate the central frequencies of PSSW modes.

dynamics is highly damped (cf. Fig. 2(c)) substantially increasing the uncertainty of the measurements.

In the frequency domain, large spin wave damping leads to overlapping PSSW peaks, as shown in Fig. 3 by solid lines with equal peak areas. The dashed curve represents the coherent sum of these Lorentzian peaks (assuming all modes are in-phase). Only the first three modes are observable above the noise floor of the experiment. Of course there are other limiting effects reducing the observed amplitude of high frequency PSSW modes namely the overlap between the spatial profile of the PSSW with that of interface-confined STT [35], the frequency spectrum of the spin current pulse, and the MOKE sensitivity depending on the PSSW mode number, as discussed in [31]. All of these factors can be modelled in detail, however this discussion is beyond the scope of this paper. Nevertheless, by comparing the experimental data to a simple analysis of the line shape presented in Fig. 3, we conclude that the main limiting factor is the enhanced magnetization damping due to spin diffusion

at large wave vectors (and frequencies).

From the above described fit, we determine the coefficient of the k_n^2 -dependent term of the effective damping, and find $\eta_{\perp} = (36.0 \pm 3.5) \cdot 10^{-3} \text{ nm}^2$. This value is about 3 times smaller than the reported values for NiFe, Co, and CoFeB [25]. The corresponding value of the transverse spin conductivity is $\sigma_{\perp} = \eta_{\perp} M_s / \gamma = 3.5 \cdot 10^{-25} \text{ Js/m}$ [16]. The simplest estimation of the transverse spin conductivity is $\sigma_{\perp} \approx (\hbar/2)^2 n_e \lambda_{\text{sd}} / (v_F m^*)$ [26], where $n_e = 1.7 \cdot 10^{29} \text{ m}^{-3}$ is the conduction electron density in Fe, $v_F = 1.98 \cdot 10^6 \text{ m/s}$ is the Fermi velocity, m^* is the effective electron mass (we use the free electron mass), and λ_{sd} is the spin diffusion length. Using literature values of λ_{sd} [38, 39], this leads to an almost one order of magnitude larger transverse spin conductivity than the value obtained in our experiments. The disagreement of the simple model with our experiment indicates the strong impact of the long-range exchange interaction due to spin transport. The latter cannot be treated as simple diffusive transport on the nm scale [21].

It should be noted, that at frequencies $f \gg 2 \text{ THz}$ the spin diffusion contribution to the magnetic damping is expected to become ineffective. Otherwise, magnetic excitations at much larger k -vectors would not be measurable. However, for iron they are clearly observable using the neutron scattering or SPEELS [27–30]. As the wavelength of the spin wave excitation becomes comparable or even smaller than the effective electron mean free path λ_e along the wave vector, the character of the spin transport changes. For electrons having energies of more than 0.3 eV above the Fermi level, we estimate λ_e to be about 2 nm [36], close to the smallest PSSW wavelength that we observe ($\lambda_{\text{min}} = 2.22 \text{ nm}$). In this case, the transport should be treated as either super-diffusive or even ballistic. The magnetization damping in this frequency region will require a different treatment of the spin transport term in Eq. (1), which is beyond the scope of this letter. Qualitatively, when the effective spin transport length approaches $\lambda/2$, the exchange of electrons between neighboring half-waves with opposite dynamical magnetization components leads to the most efficient spin wave damping. When the wavelength λ is further reduced, the diffusive spin transport effectively cancels as approximately equal numbers of half-waves with opposite dynamical magnetization components are within the effective electron mean free path λ_e . In doing so, the spin-wave relaxation due to the spin transport becomes ineffective.

In summary, we have studied damping of ultrashort terahertz-frequency PSSW modes in thin Fe films. Our results demonstrate that the dominant mechanism of dissipation in

such PSSW modes is the spin transport by itinerant electrons, which is in general either diffusive or super-diffusive. We find that at moderate wave vectors it can be treated as a transverse spin diffusion, resulting in the k_n^2 -dependence of the effective damping parameter $\alpha_{\text{eff},n}$. For the effective spin-wave damping rate this corresponds to a $\Gamma_n \sim k_n^4$ dependence. This behavior remains valid up to $k \approx 2 \text{ nm}^{-1}$ (about 2 THz frequency). By analyzing our experiments we obtain the transverse spin conductivity for Fe $\sigma_{\perp} = 3.5 \cdot 10^{-25} \text{ Js/m}$. The rapid increase of the effective damping parameter with the wave vector of the spin waves causes the damping rate to be larger than the eigenfrequency of the studied spin wave mode above the frequency $f > 1.8 \text{ THz}$. We demonstrated the dominance of spin-transport related damping for spin waves in the low THz frequency range. Using the method of coherent STT excitation the next step will be to consider spin waves at even larger wave-vectors and frequencies in ferromagnetic and antiferromagnetic materials and study the crossover from diffusive to super-diffusive or ballistic electron transport.

Acknowledgements

This work was supported by the German research foundation (DFG) through CRC/TRR 227 (project B01), the National Science Centre Poland (Grant No. 2019/35/B/ST3/00853), U.S. National Science Foundation (Grant #EFMA-1641989), by the Air Force Office of Scientific Research under the MURI grant #FA9550-19-1-0307, by the DARPA TWEED grant #DARPA-PA-19-04-05-FP-001, by the Oakland University Foundation, and by the Ministry of Education and Sciences of Ukraine (project #0121U110090).

-
- [1] M. Sparks, *Ferromagnetic Relaxation Theory* (McGraw-Hill, New York, 1964).
 - [2] A. G. Gurevich and G. A. Melkov, *Magnetization Oscillations and Waves*, vol. 1 (CRC Press, 1996), 1st ed.
 - [3] M. Sparks, R. Loudon, and C. Kittel, *Phys. Rev.* **122**, 791 (1961).
 - [4] R. Arias and D. L. Mills, *Phys. Rev. B* **60**, 7395 (1999).
 - [5] M. J. Hurben and C. E. Patton, *J. Appl. Phys.* **83**, 4344 (1998).
 - [6] Y. Tserkovnyak, A. Brataas, and G. E. W. Bauer, *Phys. Rev. Lett.* **88**, 117601 (2002).
 - [7] R. Urban, G. Woltersdorf, and B. Heinrich, *Phys. Rev. Lett.* **87**, 217204 (2001).

- [8] S. Mizukami, Y. Ando, and T. Miyazaki, *Jpn. J. Appl. Phys.* **40**, 580–585 (2001).
- [9] T. Gilbert, *IEEE Trans. Magn.* **40**, 3443 (2004), ISSN 0018-9464.
- [10] K. Gilmore and M. D. Stiles, *Phys. Rev. B* **79**, 132407 (2009).
- [11] V. Kamberský, *Czechoslovak J. Phys. B* **22**, 572 (1972).
- [12] J. Kuneš and V. Kamberský, *Phys. Rev. B* **65**, 212411 (2002).
- [13] K. Gilmore, Y. U. Idzerda, and M. D. Stiles, *Phys. Rev. Lett.* **99**, 027204 (2007).
- [14] J. Seib, D. Steiauf, and M. Fähnle, *Phys. Rev. B* **79**, 092418 (2009).
- [15] D. Steiauf, J. Seib, and M. Fähnle, *Phys. Rev. B* **78**, 020410(R) (2008).
- [16] R. Verba, V. Tiberkevich, and A. Slavin, *Phys. Rev. B* **98**, 104408 (2018).
- [17] V. G. Bar'yakhtar, *Sov. Phys. JETP* **60**, 863 (1984), [*Zh. Eksp. Teor. Fiz.* 87, 1501 (1984)].
- [18] V. G. Bar'yakhtar and A. G. Danilevich, *Low Temp. Phys.* **39**, 993 (2013).
- [19] E. M. Hankiewicz, G. Vignale, and Y. Tserkovnyak, *Phys. Rev. B* **78**, 020404 (2008).
- [20] J. Foros, A. Brataas, Y. Tserkovnyak, and G. E. W. Bauer, *Phys. Rev. B* **78**, 140402 (2008).
- [21] Y. Tserkovnyak, E. M. Hankiewicz, and G. Vignale, *Phys. Rev. B* **79**, 094415 (2009).
- [22] C. H. Wong and Y. Tserkovnyak, *Phys. Rev. B* **80**, 184411 (2009).
- [23] S. Zhang and S. S.-L. Zhang, *Phys. Rev. Lett.* **102**, 086601 (2009).
- [24] W. Wang, M. Dvornik, M.-A. Bisotti, D. Chernyshenko, M. Beg, M. Albert, A. Vansteenkiste, B. V. Waeyenberge, A. N. Kuchko, V. V. Kruglyak, et al., *Phys. Rev. B* **92**, 054430 (2015).
- [25] Y. Li and W. E. Bailey, *Phys. Rev. Lett.* **116**, 117602 (2016).
- [26] H. T. Nembach, J. M. Shaw, C. T. Boone, and T. J. Silva, *Phys. Rev. Lett.* **110**, 117201 (2013).
- [27] K. Zakeri, Y. Zhang, J. Prokop, T.-H. Chuang, N. Sakr, W. X. Tang, and J. Kirschner, *Phys. Rev. Lett.* **104**, 137203 (2010).
- [28] J. Prokop, W. Tang, Y. Zhang, I. Tudosa, T. Peixoto, K. Zakeri, and J. Kirschner, *Phys. Rev. Lett* **102**, 177206 (2009).
- [29] G. Shirane, V. J. Minkiewicz, and R. Nathans, *Journal of Applied Physics* **39**, 383 (1968).
- [30] H. Mook and R. Nicklow, *Phys. Rev. B* **7**, 336 (1973).
- [31] See the Supplemental Material at [URL] for discussions of the dispersion relation for FMR mode and PSSWs, the spin wave ellipticity coefficient and minor contributions to the effective damping model, which includes Refs. [2, 32, 40–42].
- [32] L. Brandt, U. Ritzmann, N. Liebing, M. Ribow, I. Razdolski, P. Brouwer, A. Melnikov, and

- G. Woltersdorf, arXiv:2106.01066 (2021).
- [33] A. Melnikov, I. Razdolski, T. O. Wehling, E. T. Papaioannou, V. Roddatis, P. Fumagalli, O. Aktsipetrov, A. I. Lichtenstein, and U. Bovensiepen, *Phys. Rev. Lett* **107**, 076601 (2011).
- [34] A. Alekhin, I. Razdolski, N. Ilin, J. P. Meyburg, D. Diesing, V. Roddatis, I. Rungger, M. Stamenova, S. Sanvito, U. Bovensiepen, et al., *Phys. Rev. Lett.* **119**, 017202 (2017).
- [35] I. Razdolski, A. Alekhin, N. Ilin, J. P. Meyburg, V. Roddatis, D. Diesing, U. Bovensiepen, and A. Melnikov, *Nat. Comm.* **8**, 15007 (2017).
- [36] A. Melnikov, L. Brandt, N. Liebing, M. Ribow, I. Mertig, and G. Woltersdorf, arXiv:2106.15533 (2021).
- [37] B. Heinrich, G. Woltersdorf, R. Urban, and E. Simanek, *J. Appl. Phys.* **93**, 7545 (2003).
- [38] A. A. Starikov, P. J. Kelly, A. Brataas, Y. Tserkovnyak, and G. E. W. Bauer, *Phys. Rev. Lett.* **105**, 236601 (2010).
- [39] K.-H. Ko and G.-M. Choi, *J. Magn. Magn. Mater.* **510**, 166945 (2020).
- [40] A. Hallal, H. X. Yang, B. Dieny, and M. Chshiev, *Phys. Rev. B* **88**, 184423 (2013).
- [41] H. Yang, M. Chshiev, B. Dieny, J. Lee, A. Manchon, and K. Shin, *Phys. Rev. B* **84**, 054401 (2011).
- [42] M. L. M. Laliou, P. L. J. Helgers, and B. Koopmans, *Phys. Rev. B* **96**, 014417 (2017).